Proceedings of GPPS Forum 18
Global Power and Propulsion Society
Montreal, 7th-9th May 2018
www.gpps.global

GPPS-2018-47

# OPTIMIZATION OF HIGH SUBSONIC, HIGH REYNOLDS NUMBER AXIAL COMPRESSOR AIRFOIL SECTIONS FOR INCREASED OPERATING RANGE

**Daniel Giesecke, Marcel Bullert, Jens Friedrichs**
**TU Braunschweig**
Institute of Jet Propulsion and Turbomachinery
d.giesecke@ifas.tu-braunschweig.de
Braunschweig, Germany

**Udo Stark**
**TU Braunschweig**
Institute of Fluid Mechanics
Braunschweig, Germany

## ABSTRACT

In this paper an increase of up to 4 % in surge margin while having more than a one percent increase in peak isentropic efficiency for an optimized stator of a high subsonic axial compressor was achieved. Using a simplified design method coupled with an optimization algorithm, only stacked stator spanwise blade elements were optimized and remaining the same rotor.

Subsonic axial compressor can be exposed to different inflow situations along blade height with circumferential changes. In the present study, the optimization of each airfoil section is done by only varying three main parameters, which reduces computational time. The chosen approach combines a generalized parabolic arc mean camber with the so-called Class Function / Shape Function Methodology.

The comparison to the original stator airfoil sections shows an increase in operating range of up to 22 % with 33 % lower minimum losses. A stator only investigation confirms the increased performance for all optimized airfoil sections.

## INTRODUCTION

In recent years, several optimization methods for turbomachinery blade profiles have been developed. This includes parameterized airfoil sections with spline functions coupled with a normal-distributed random search code and a gradient method with the two-dimensional blade-to-blade flow solver MISES (Koeller et al., 1999). An increase of stall margin with lower pressure losses over the entire larger operating range was observed in comparison to controlled diffusion airfoils. In experimental investigations the widening in low-loss operating range and increased stall margin for those high Reynolds numbers airfoils were confirmed by Kuester et al. (1999).

Similar achievements were made by Sieverding et al. (2004) with a genetic algorithm. For profile generation two fourth order Bezier splines with two linear functions as camber line for profile generation were utilized. Again, the flow solver MISES was implemented within the optimization procedure. Both approaches share a large number of geometric parameters for optimization, which is, in general, widely used in profile optimization techniques.

In Giesecke et al. (2017) a geometry parameterization technique combined MISES and a single-objective genetic optimization algorithm with a suitable objective function. The geometry definition consists of a generalized parabolic arc line (Schlichting and Truckenbrodt, 1979) and the so-called Class Function / Shape Function Methodology (CSM) based on Kulfan and Bussoletti (2006) for aircraft shapes as a thickness distribution. Furthermore, in a comparison with high-performance profiles of the above-mentioned literature, a close agreement was shown. This approach results in a profile shape defined by only three optimization parameters and enables designs with large operating ranges.

The developed airfoils were designed for modern compressor middle and end stages of industrial gas turbines, which operate at high Reynolds numbers and moderate subsonic Mach number. The corresponding Reynolds number is in the order of 2 to 6 x $10^6$. This is much higher compared to aero engine profile, which operate at Reynolds number of about 0.6 to 1.2 x $10^6$ (Schreiber et al., 2000).

The present study aims at applying the chosen approach on profiles operating at large Reynolds number. In particularly, the stator airfoil sections of a high subsonic, high Reynolds number axial compressor are optimized and the resulting stage performance is presented.

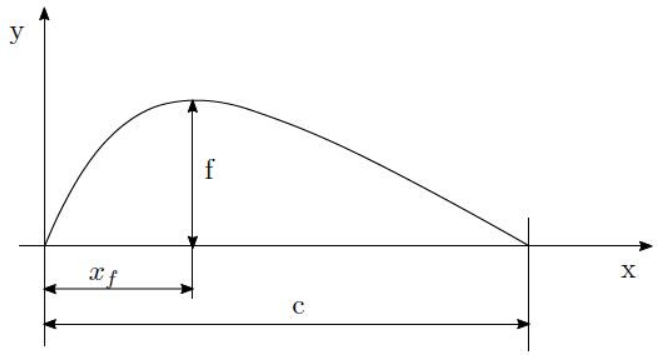


**Figure 1 Camber Line Parameters**

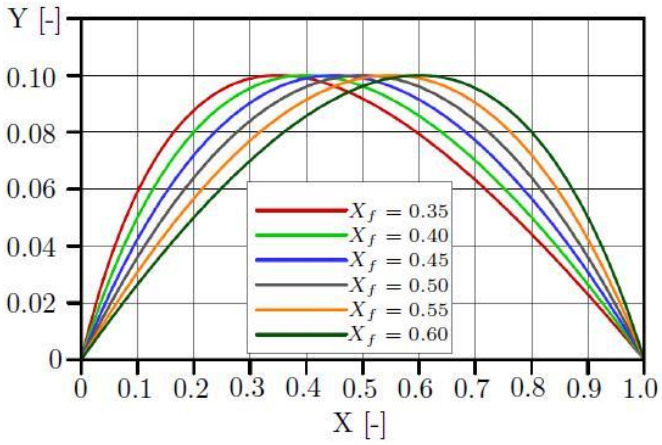


**Figure 2 Camber Lines of Max. Camber f / c = 0.1 at various Chordwise Positions**

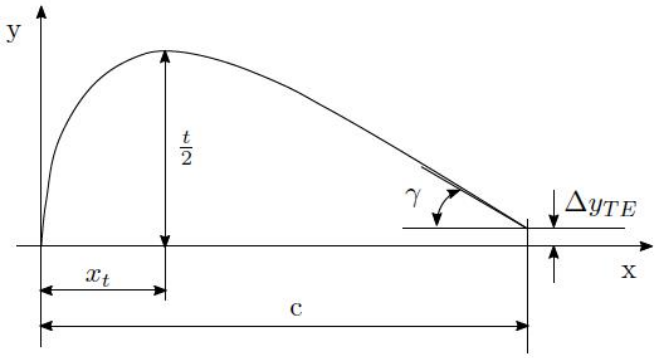


**Figure 3 Thickness Parameters**

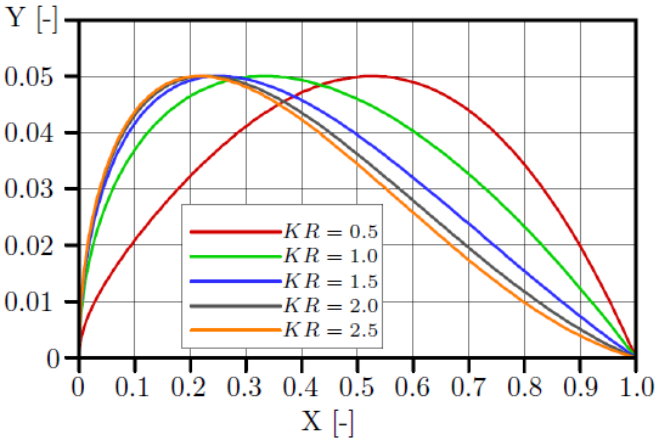


**Figure 4 Thickness Distributions of Max. Thickness t / c = at various Chordwise Positions**

## METHODS

### Blade Section Geometry

*Camber Lines*

The challenge for the geometry method is to produce a fast analytical procedure with a small number of parameters for the design of high subsonic (below critical Mach number), high Reynolds number compressor blade sections. The section shapes are obtained by superimposing a camber line and a thickness distribution. Both the camber line and the thickness distributions are prescribed by analytical functions to cut down the CPU-time for geometry set up and to guarantee smooth geometries.

The camber lines are so-called generalized parabolic arc lines (Schlichting and Truckenbrodt, 1967) of the form

$$Y_c(X) = a \cdot \frac{X(1-X)}{1+bX} \qquad (1)$$

with a and b representing the following abbreviations

$$a = \frac{1}{X_f^2}\frac{f}{c} \qquad \text{and} \qquad b = \frac{1-2X_f}{X_f^2}.$$

with parameters f / c as maximum ordinate (expressed as fraction of chord) and $X_f$ as chordwise position of the maximum ordinate, see Figure 1. In Figure 2 an evaluation of the above formula for f / c = 0.1 and various values of the chordwise position $X_f$ of the maximum ordinate is shown.

*Thickness Distributions*

The thickness distributions, as seen in Figure 3, are derived from the following formulas representing the Class Function / Shape Function Methodology (Kulfan and Bussoletti, 2006) in its simplest form (scaling factor omitted)

$$Y_t(X) = C(X) \cdot S(X) + X \cdot \Delta Y_{TE}. \qquad (2)$$

with Class Function

$$C(X) = \sqrt{X} \cdot (1 - X). \qquad (3)$$

and Shape Function

$$S(X) = KR \cdot (1 - X) + \frac{1}{KR} \cdot X, \qquad (4)$$

where KR is a shape parameter determining the leading edge radius $R_{LE}$

$$S(0) = \sqrt{2R_{LE}}, \qquad (5)$$

the trailing edge angle $\gamma$

$$S(1) = \tan\gamma + \Delta Y_{TE} \qquad (6)$$

and the maximum thickness location $X_t$

$$Y_t'(X_t) = \sqrt{X_t} \cdot (1 - X_t) \cdot S'(X_t) + \left[-\sqrt{X_t} + \frac{1-X_t}{2\sqrt{X_t}}\right] \cdot S(X_t) + \Delta Y_{TE} \quad (7)$$
$$= 0.$$

An evaluation of the above formulas for t / c = 0.1, $\Delta Y_{TE} = 0$ and various values of the shape parameter KR is presented in Figure 4.

Altogether, the geometry model has finally only three parameters: two for the camber line and one for the thickness distribution for each blade design.

### Blade-to-Blade Flow Solver

The blade-to-blade flow solver MISES 2.63 (Drela and Youngren, 2008) has been selected as the flow code for the optimization. This code describes the inviscid flow using the steady Euler equations (Giles, 1985), while the viscous effects are modelled by the integral boundary layer equations (Drela, 1986). The coupled system of nonlinear equations is solved by a Newton technique. The boundary conditions are defined by those of the cascade to be designed and optimized. The design inlet Mach number is kept constant while the inlet angle is varied between positive and negative stall. Boundary layer transition is predicted using the criterion of Abu-Ghannam / Shaw (1980) in a slightly modified version (Drela, 1998) to achieve a better modelling of the flow physics at transition.

The solver has been sufficiently validated for cascade flows at low and high Reynolds numbers, (Schreiber et al., 2004; Sonoda and Schreiber, 2007) and (Koeller, 1999; Benini and Toffolo, 2002) respectively, and at various turbulence levels with and without turbulence grids (Schreiber, 2000). AVDR effects are taken into account by a hyperbolic tangent variation of the streamtube thickness (Stark and Hoheisel, 1981; Stark, 1987).

Cascade data is used for the boundary conditions within the solver. After grid generation, the design inlet Mach number is kept constant and the inlet angle is varied between choke and stall.

### Optimization Method

As mentioned above, only three parameters need to be optimized: two for the camber line and one for the thickness distribution for each stator section.

In the present paper, the single-objective genetic algorithm (SOGA) from the DAKOTA library (Adams et al., 2014) starts with 100 samples of random profiles. Those profiles were evaluated by an objective function and passed or not passed to the next generation. The latter were rejected based on the specific limit according to the exit flow angle $\beta_2$. In the mutation phase up to 5000 individuals in maximum 250 generations are produced and evaluated as described. A genetic algorithm was chosen in this study due to the great improvements made by Sieverding et al. (2004) with a similar algorithm type.

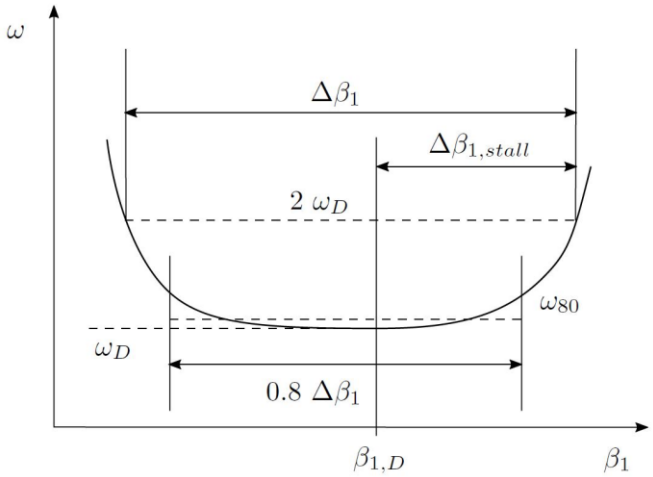


**Figure 5 Parameters of the Objective Function, adapted from Sieverding et al. (2004)**

In the present study, an objective function reported by Koeller (1998) and Sieverding et al. (2004) was applied, which is defined as follows

$$OBF = C_1\left(\frac{\omega_D}{\omega_{D,ref}}\right) + C_2\left(\frac{\Delta\beta_{1,ref}}{\Delta\beta_1}\right) + C_3\left(\frac{\Delta\beta_{1,stall,ref}}{\Delta\beta_{1,stall}}\right) + C_4\left(\frac{\omega_{80}}{\omega_{80,ref}}\right) + C_5\left(\frac{\sigma_{80}}{\sigma_{80,ref}}\right). \quad (7)$$

The objective function consists of five components each one with its own weighting factor ($C_1 = 1$, $C_{2,4,5} = 0.5$ and $C_3 = 2$). Further to that, each component is normalized by a corresponding value of a reference profile. Figure 5 shows an illustration of the theory behind the objective function and of its components. The operating range $\Delta\beta_1$ is determined by twice the value of the loss coefficient $\omega_D$ at design inlet angle $\beta_{1,D}$. The stall margin $\Delta\beta_{1,stall}$ is known to be the distance from design inlet angle $\beta_{1,D}$ to the stall angle. In order to generate an airfoil, which also operates at low loss level in case of small deviations from design angle, the average loss of the inner 80 % of the operating range $\omega_{80}$ and its standard deviation $\sigma_{80}$ is also implemented.

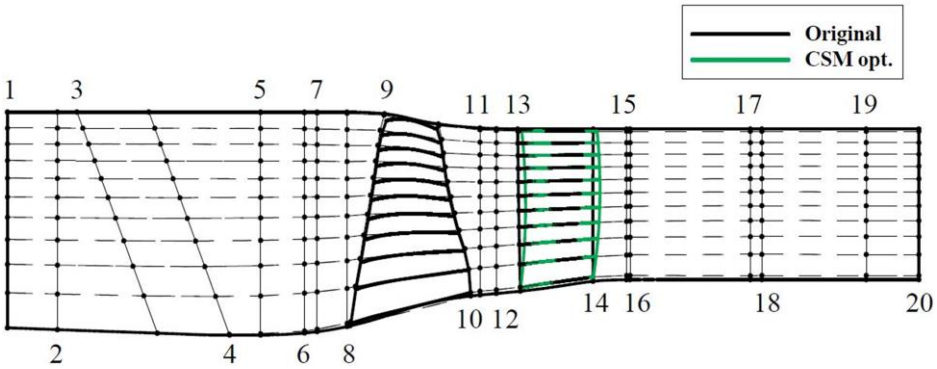


**Figure 6 Meridional View of NASA Stage 67**

### Stage Performance Calculation

Based on the data in Hathaway (1986), the numerical setup shown in Figure 6 was set up. The original profile data were projected on the streamlines. At each station (1 to 20) for each streamline experimental data is given in Hathaway (1986). In this study, pressure and temperature from the experimental data from station 1 and 20 were used as in- respectively outlet condition for the numerical setup. The 3D blade geometry was generated by stacking the eleven profiles for each blade along its center of gravity. After generating the 3D geometry, the commercial semi-automatic grid generator NUMECA Autogrid 5 was used for mesh generation of the stage equivalent to Figure 6. The grid sensitivity study (evaluation of mass flow, pressure ratio and stage efficiency) led to 5.1 million nodes for the whole domain including one rotor and two stator blades. Summarizing the grid criteria, a minimum skewness angle of 19°, maximum aspect ratio of 3000 and maximum expansion ratio of 2.4 was reached.

The commercial solver ANSYS CFX 17.0 was used for the 3D Reynolds-averaged Navier-Stokes (3D-RANS) simulations with the k-ω turbulence model. The domain was simulated with pitch periodic boundaries. On each surface in the numerical setup no hydraulic smooth walls were applied. The mixing plane between rotor and stator domain averages the velocity. Full convergence was achieved with RMS residuals below $10^4$. The maximum dimensionless wall distance $y^+$ for all walls, rotor and stator blades were around 1.3 for the design speed line.

### RESULTS

For comparison purposes a high subsonic axial compressor available in the open literature was chosen, which is well-known as the NASA stage 67 (Hathaway, 1986) and named in this paper as the original configuration. The optimized stator airfoil sections by using the Class Function / Shape Function Methodology are referred in the present paper as CSM opt. The rotor blade remains the same for both configurations.

**Table 1 Stage Design Parameter**

| Design point objectives | Formula | Value |
|---|---|---|
| Mass flow (corrected) | $\dot{m}_{red}$ | 32.25 kg/sec |
| Total pressure ratio | $PR$ | 1.59 |
| Hub / tip ratio | | |
| - rotor in- / outlet | $v$ | 0.375 / 0.478 |
| - stator in- / outlet | | 0.5 / 0.53 |
| Casing diameter | $D_c$ | 244 mm |
| Tip clearance | $s$ | 0.5 mm |
| Rotational speed | $n$ | 16048.2 1/min |

The original rotor comprises 22 and the stator 34 blades of multiple (rotor airfoils) respectively double (stator airfoils) circular arc (DCA) profiles. At design condition the total pressure ratio, corrected mass flow and rotary speed is 1.59, 32.25 kg/sec and 16048.3 1/min. Table 1 summarizes the stage design parameter. All eleven stator blade profiles were optimized. The numerical domain used in MISES for the optimisation starts from station 12 to 16, see Figure 6. The change in 3D geometry is observable in the meridional view in Figure 6.

Figure 7 to 9 show the change of the three optimization parameters position of maximum camber, maximum camber and position of maximum thickness for the original and for the optimized stator configuration. The change of the position of maximum camber and thickness is clearly observable. The optimization process moves both values towards leading edge and the position of maximum thickness to a greater extent. This leads to a more front loaded profile as shown in Figure 10 for the mid section profile. This is in accordance to previous investigations made by Koeller et al. (1999) and Giesecke et al. (2017). The airfoils are stacked radially in its center of gravity and therefore, the 3D blade geometry changes as indicated in Figure 6. This leads to swept blade geometry mainly due to position of maximum camber and thickness.

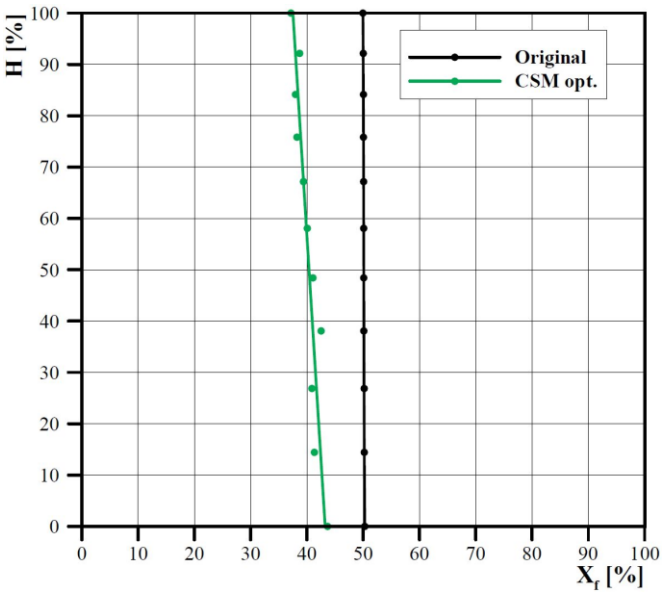


**Figure 7 Change of Position of Maximum Camber**

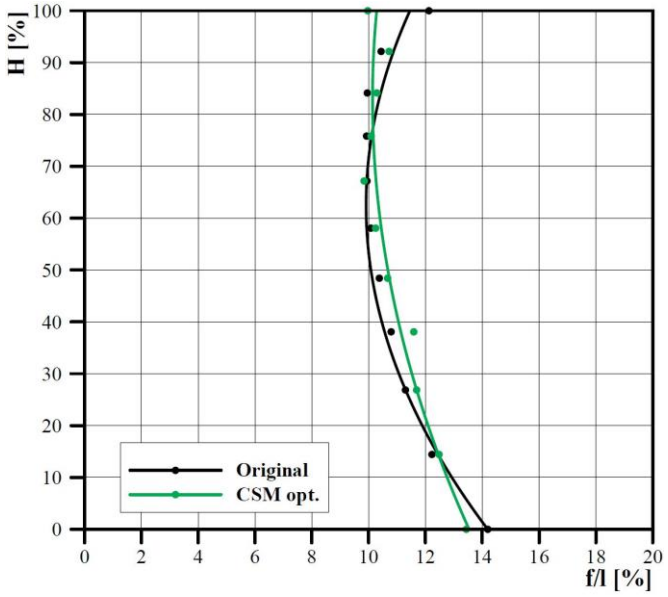


**Figure 8 Change of Maximum Camber**

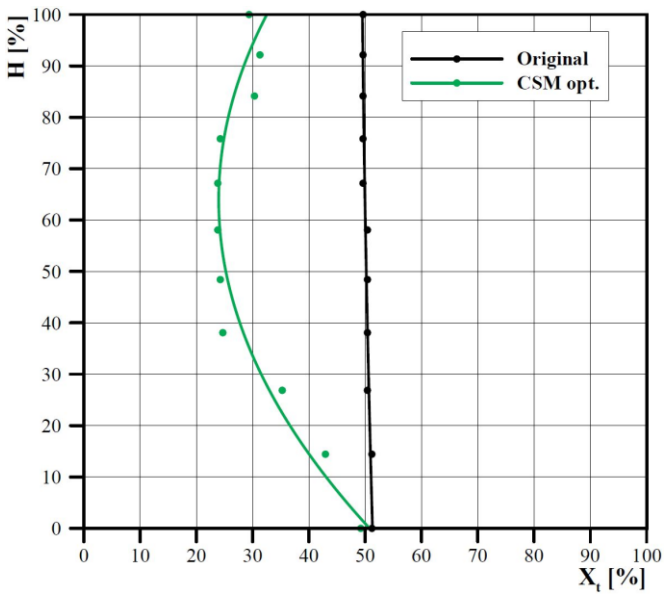


**Figure 9 Change in Position of Maximum Thickness**

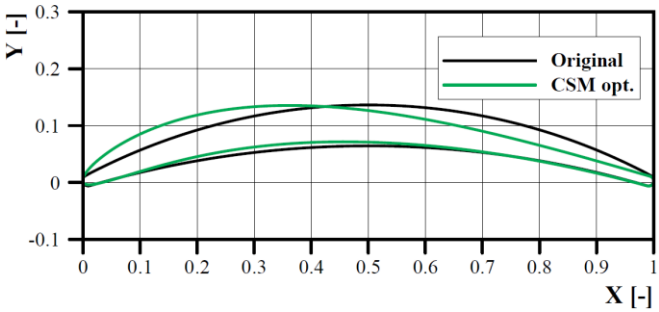


**Figure 10 Original and Optimized Mid Sections in Comparison**

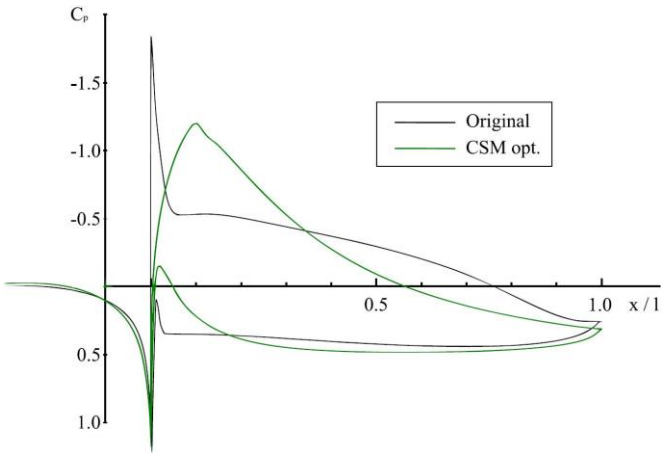


**Figure 11 Mid Sections Pressure Distributions at Design Inlet Angle**

### Stator Mid Sections

In this section, the stator airfoil design and geometric parameters at midspan are shown as example. The design specifications and main parameters for the original and CSM optimized section are documented in Table 2. The design specifications of the stator mid section appear in the first column in particularly the Mach number $Ma_1 = 0.644$, the blade turning $\Delta\beta_1 = 39.6°$ at the Reynolds number $Re_1 = 1.07 \times 10^6$. The second column shows the original section parameters. The optimization starts with an initial CSM airfoil (not shown here), which has been matched to fit with the original airfoil and has been taken for the reference values in eq. (7) for the objective function. Obviously, the parameters of the initial CSM airfoil sections are in agreement with the original stator section parameters. In the last column, the main geometric parameters for the optimized CSM ($X_f$, f / c and $X_t$ (KR)) profile are presented. All profiles are shown in Figure 10. Both, the position of maximum camber $X_f$ and maximum thickness $X_t$ are moved

**Table 2 Stator Mid Sections**

| Design Specifications | | | Original (DCA) | | | | $CSM_{opt.}$ |
|---|---|---|---|---|---|---|---|
| $Ma_1$ | = | 0.644 | $X_f$ | = | 0.5 | → | 0.41 |
| $Re_1$ | = | $1.07 \times 10^6$ | f / c | = | 0.101 | → | 0.103 |
| $\beta_1$ | = | 39.6° | $X_t$ | = | 0.5 | → | 0.24 |
| $\beta_2$ | = | 0° | | | | | KR = 2.5 |
| t / c | = | 0.62 | $\lambda$ | = | 13.6° | | |
| $t_1$ | = | $0.5 \times 10^{-3}$ | | | | | |
| AVDR | = | 1.077 | | | | | |
| $Tu_1$ | = | 3 % | | | | | |

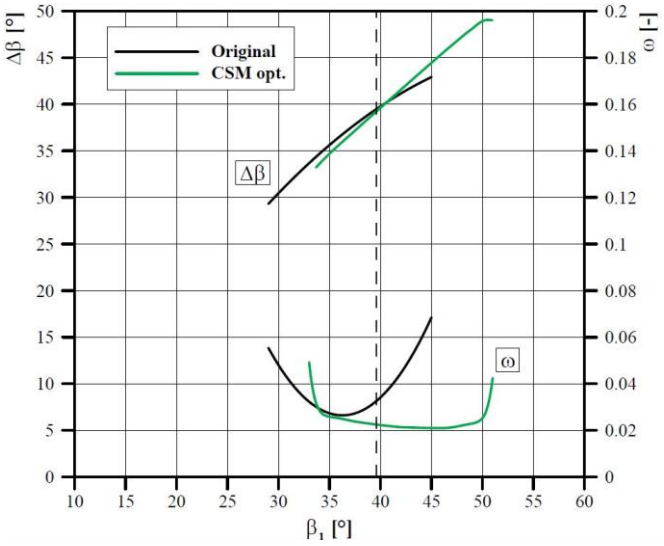


**Figure 12 Mid Sections Overall Performance Characteristics**

towards the leading edge for the optimised case. The optimized profile has reduced leading edge sharpness, which results in smooth suction side acceleration until the maximum Mach number at around 10 % chord length is reached, see Figure 11. The deceleration starts with a steep gradient, followed by a small separation bubble and becoming increasingly smaller towards the trailing edge. This is significantly different compared to the original profile. It shows the front loaded character with controlled diffusion towards the trailing edge, where the front part of the blade has the thinnest boundary layer and therefore, the strong acceleration is less negatively affected. This has also been reported by Casey (1994). Hence, the operating range increases by 9 % with larger distance to stall, see Figure 12, when comparing with the original section. The minimum loss decreases by 34 % as a result of the smooth curvature with the controlled diffusion towards the trailing edge.

## Stator Performance

The total pressure recovery factor $p_{t,st.out} / p_{t,st.in}$ reaches unity in case of ideal flow condition. In Robbins et al. (1965), the procedure for calculating the blade-element efficiency is described by using the ratio of stage efficiency to rotor efficiency and the rotor total pressure ratio $p_{t,st.out} / p_{t,st.in}$. This expression is then derived from the following equation

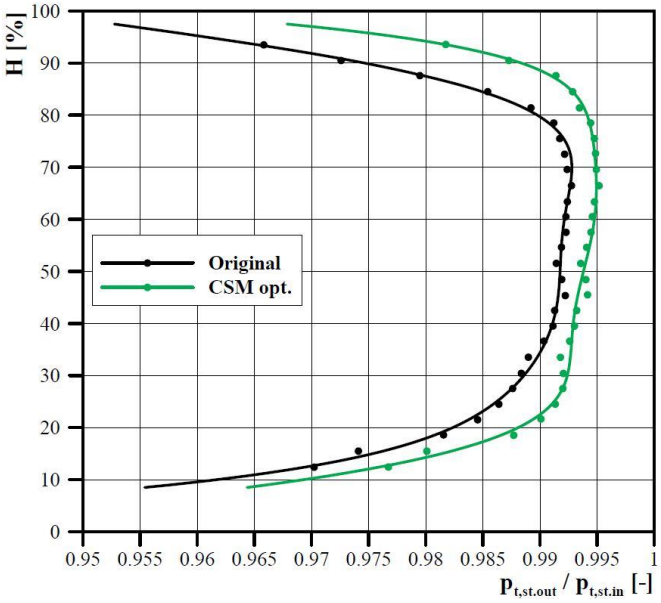


**Figure 13 Stator Recovery Factor at Design Mass Flow**

$$\frac{p_{t,st.out}}{p_{t,st.in}} = 1 - \omega_{st}\left[1 - \left(1 + \frac{\kappa-1}{2} Ma_{st.in}^2\right)^{-\frac{\kappa}{\kappa-1}}\right], \quad (9)$$

where $\omega_{st}$ is the stator loss coefficient and $Ma_{st.in}$ the stator Mach number in absolute frame of reference.

The so-called stator recovery factor is shown in Figure 13. It is observable that the CSM optimized profiles are in average more closely to unity compared to the original stator configuration meaning that the stator pressure recovery is larger.

As expected from Figure 13, the CSM optimized profiles obtain the highest average value with 0.991 while the original reaches 0.986 in average. Therefore, the effectiveness of the stator profile optimization is confirmed and it may be concluded that the optimized stator contributes to a large proportion for a rise in stage performance.

## Stage Performance

Each blade for each profile generation type has been stacked in a similar manner to perform numerical investigations by using ANSYS CFX 17.0. For all two cases the corresponding characteristic line has been calculated. The results of the numerical simulation are illustrated in

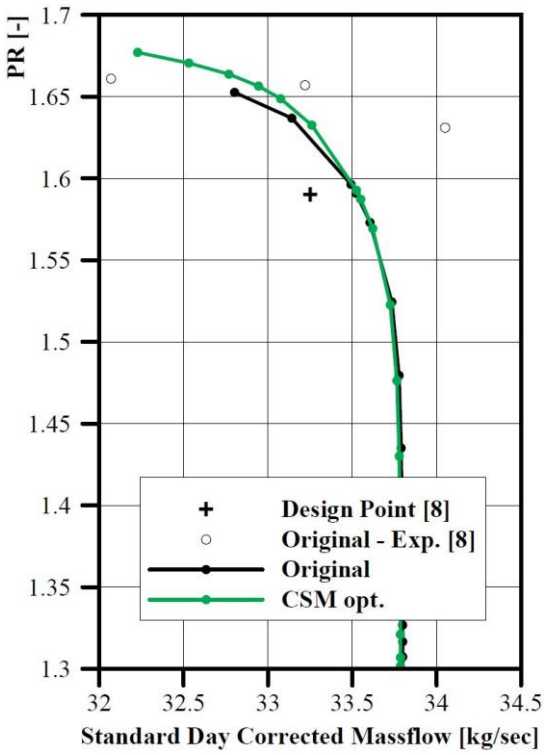


**Figure 14 Stage PR Characteristics**

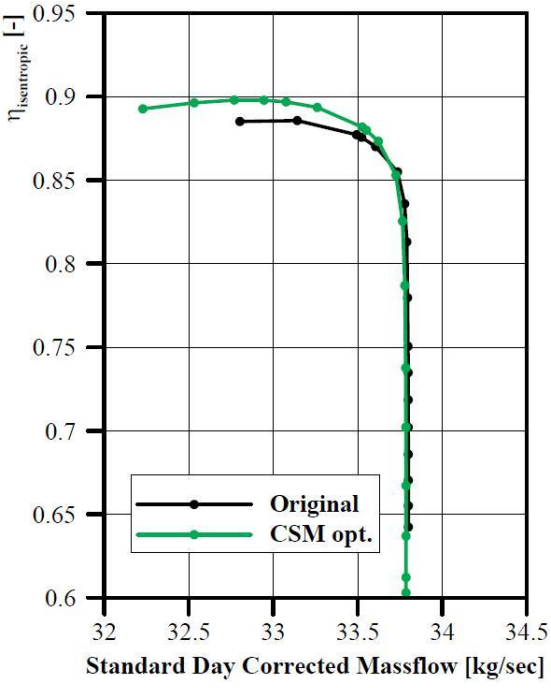


**Figure 15 Stage Isentropic Efficiency Characteristics**

Figure 14 for PR and in Figure 15 for isentropic efficiency. The stage pressure ratio and isentropic efficiency against standard day corrected mass flow is shown there.

Besides, the design point and experiments given in Hathaway (1986) are included in Figure 14 as well. In the experiments the blades are exposed to centrifugal forces, which results in a decrease of stagger angle and hence, an opening of the passage. Therefore, the mass flow through the stage increases, which is also reported in Bölcs and Suter (1986). This explains the difference between the experimental and numerical results.

In order to estimate the stage performance the surge margin is a very good indicator. In Bräunling (2009) the commonly used surge margin is defined as

$$\Delta SM_{PR} = \frac{PR_{stall} - PR_{DP}}{PR_{DP} - 1} \cdot 100\%. \quad (8)$$

**Table 3 Compressor Performance Parameter**

| | Unit | Original | CSM opt. |
|---|---|---|---|
| $\Delta SM_{PR}$ | [%] | 10.7 | 14.8 |
| $\eta_{isentropic,peak}$ | [%] | 88.6 | 89.8 |

As indicated in Table 3, the surge margin based on the pressure ratio of the optimized configuration increases by 4.1 % in contrast to the original stator. It is worth noting, that DCA airfoils as used in the original configuration are a common way to specify stator blades (Cumpsty, 1989). The rise in isentropic efficiency is in a good agreement with regards to the mean section performance evaluation, where the operating range of the profile increases by 9 %.

Further to that, the peak isentropic efficiency shows an increase as well of more than one percent than the original stage configuration.

## CONCLUSIONS

To summarize, a profile generation method for the stator of a high subsonic, high Reynolds number axial compressor stage has been presented. This method combines an optimization with a geometry definition consisting of a small number of variables and was applied on all stator airfoil sections.

The optimized mid section show an increase of 9 % in operating range and a decrease of 34 % in peak minimum losses. The main focus of this paper is the assessment of the prescribed design method in terms of compressor stage performance and in particular of stator recovery factor to estimate the complete benefits. With regards to stage performance the surge margin has been increased by 4.1 % when comparing to the original stage configuration. This is a satisfactory achievement bearing in mind that 15 % stall margin is required to assure a safe operation. As a consequence of the controlled diffusion behaviour of the optimized profiles, the peak isentropic efficiency rises by more than one percentage point. Finally, the evaluation of the stator recovery factor indicates that the optimized profiles are able to achieve higher values along the blade height in contrast to the original stator.

Future research should focus on the optimization weighting factors in terms of the design method. However, on the other hand experimental investigations are required to confirm the numerical outcome. Moreover, in the on-going research project, the application to aero engine stators should be pursued to achieve a favourable effect in case of inflow distortion.

## NOMENCLATURE

### Latin Symbols

| | |
|---|---|
| a, b | parabolic mean arc line parameter |
| c | chord |
| C | Class Function |
| $C_1 – C_5$ | weighting factor |
| f | camber |
| $D_c$ | casing diameter |
| KR | shape parameter |
| $\dot{m}_{red}$ | corrected mass flow |
| Ma | Mach number |
| *n* | rotational speed |
| p | pressure |
| *PR* | pressure ratio |
| *s* | tip clearance |
| t | thickness |
| Re | Reynolds number |
| $R_{LE}$ | leading edge radius |
| S | Shape Function |
| SM | surge margin |
| T | maximum thickness |
| Tu | turbulence level |
| X | x value |
| $X_t$ | position of maximum thickness |
| $X_f$ | position of maximum camber |
| Y | y value |
| $Y_c$ | camber line |
| $Y_t$ | thickness |
| $Y_{TE}$ | trailing edge thickness |

### Greek Symbols

| | |
|---|---|
| β | flow angle |
| γ | trailing edge angle |
| Δ | difference |
| η | efficiency |
| κ | isentropic exponent |
| λ | stagger angle |
| ν | hub / tip ratio |
| σ | standard deviation |
| ω | total pressure loss coefficient |

### Subscripts

| | |
|---|---|
| ‘ | derivative |
| D | design |
| DP | design point |
| in | inlet |
| opt. | optimized |
| out | outlet |
| PR | pressure ratio |
| ref | reference |
| st. | stator |
| stall | stall margin |
| t | total |
| 1 | inlet |
| 2 | outlet |
| 80 | 80 % of operating range |

### Abbreviations

| | |
|---|---|
| AVDR | axial velocity density ratio |
| CFD | computational fluid dynamics |
| CSM | Class Function / Shape Function Methodology |
| DCA | double circular arc |
| OBF | objective function |
| RANS | Reynolds-averaged Navier-Stokes |
| SOGA | single-objective genetic algorithm |

## ACKNOWLEDGMENTS

The authors gratefully acknowledge the funding as part of the Coordinated Research Centre 880 (Sonderforschungsbereich 880, SFB 880) provided by the German Research Foundation (Deutsche Forschungsgemeinschaft, DFG).

## REFERENCES

[1] Koeller, U., Moenig, R., Kuesters, B., and Schreiber, H. A. (1999). Development of advanced compressor airfoils for heavy-duty gas turbines - part I: Design and optimization. J. Turbomachinery 122 (3), 1999, 397-405. doi:10.1115/99-GT-095

[2] Kuesters, B., Schreiber, H. A., Koeller, U., and Moenig, R. (1999). Development of advanced compressor airfoils for heavy-duty gas turbines - part II: Experimental and theoretical analysis. J. Turbomachinery 122 (3), 406-414. doi:10.1115/99-GT-096

[3] Sieverding, F., Ribi, B., Casey, M., and Meyer, M. (2004). Design of industrial axial compressor blade sections for optimal range and performance. J. Turbomachinery 122 (2), 323-331. doi:10.1115/1.1737782

[4] Giesecke, D., Stark, U., Harms García, R., and Friedrichs, J. (2017). Design and Optimization of Compressor Airfoils by Using Class Function / Shape Function Methodology. 17th International Symposium on Transport Phenomena and Dynamics of Rotating Machinery (ISROMAC).

[5] Schlichting, H., and Truckenbrodt, E. (1979) Aerodynamics of the Airplane (Translated by H. J. Ramm). McGraw-Hill International Book Company.

[6] Kulfan, B. M., and Bussoletti, J. E. (2006). Fundamental parametric geometry representations for aircraft component shapes. AIAA Paper 2006-6948, 1-45.

[7] Schreiber, H. A., Steinert, W., and Kuesters, B. (2000). Effects of Reynolds number and freestream turbulence on boundary layer transition in a compressor cascade. J. Turbomachinery, 124 (1), 1-9. doi:10.1115/1.1413471

[8] Hathaway, M. D. (1986). Unsteady Flows in a Single-Stage Transonic Axial-Flow Fan Stator Row. NASA TM 88929.

[9] Drela, M., and Youngren, H. (2008). A User's Guide to MISES 2.63. MIT Aerospace Computational Design Lab.

[10] Giles, M. B. (1985). Newton solution of steady two-dimensional transonic flow. GTL Report No. 186.

[11] Drela, M. (1986). Two-dimensional transonic aerodynamic design and analysis using the Euler equations. GTL Report No. 187.

[12] Abu-Ghannam, B. J., and Shaw, R. (1980). Natural transition of boundary layers-the effects of turbulence,

pressure gradient, and flow history. J. Mechanical Engineering Science, 22 (5), 213-228. doi:10.1243/JMES_JOUR_1980_022_043_02
[13] Drela, M. (1998). MISES Implementation of Modified Abu-Ghannam / Shaw Transition Criterion (Second Revision). MIT Aero-Astro.
[14] Schreiber, H. A., Steinert, W., Sonoda, T., and Arima, T. (2004). Advanced high-turning compressor airfoils for low Reynolds number condition - part II: Experimental and numerical analysis. J. Turbomachinery, 126 (4), 482-492. doi:10.1115/1.1737780
[15] Sonoda, T., and Schreiber, H. A. (2007). Aerodynamic characteristics of supercritical outlet guide vanes at low Reynolds number conditions. J. Turbomachinery, 129 (4), 694-704. doi:10.1115/1.2720868
[16] Koeller, U. (1998). Entwicklung einer fortschrittlichen Profilsystematik fuer stationaere Gasturbinenverdichter. PhD thesis, Ruhr-Universität Bochum, DLR 1999-20.
[17] Benini, E., and Toffolo, A. (2002). Development of high-performance airfoils for axial flow compressors using evolutionary computation. J. Propulsion and Power, 18 (3), 544-554. doi:10.2514/2.5995
[18] Stark, U., and Hoheisel, H. (1981). The combined effect of axial velocity density ratio and aspect ratio on compressor cascade performance. J. Engineering for Power, 103 (1), 247-255. doi:10.1115/1.3230704
[19] Stark, U. (1987). Ebene Verdichtergitter in quasi zweidimensionaler Unterschallströmung. VDI Forschungsheft 641/87, 247-255.
[20] Adams, B. M., Bauman, L. E., Bohnho, W. J., Dalbey, K. R., Ebeida, M. S., Eddy, J. P., Eldred, M.S., Hough, P. D., Hu, K. T., Jakeman, J. D., Stephens, J.A., Swiler, L. P., Vigil, D. M., and Wildey, T. M. (2014). Dakota, A Multilevel Parallel Object-Oriented Framework for Design Optimization, Parameter Estimation, Uncertainty Quantification, and Sensitivity Analysis: Version 6.4 User's Manual, Sandia Technical Report SAND2014-4633.
[21] Casey, M. V. (1994). The industrial use of CFD in the design of turbomachinery. AGARD Lecture Series 195.
[22] Bölcs, A., and Suter, P. (1965). Transsonische Turbomaschinen. Wissenschaft und Technik.
[23] Braeunling, W. J. G. (2009). Flugzeugtriebwerke - Grundlagen, Aero-Thermodynamik, ideale und reale Kreisprozesse, Thermische Turbomaschinen, Komponenten, Emissionen und Systeme. Springer-Verlag, 3. edition.
[24] Robbins, W. H., Jackson, R. J., and Lieblein, S. (1965). “Blade-element flow in annular cascades” in: Aerodynamic Design of Axial-Flow Compressors - NASA SP-36, 227-254.
[25] Cumpsty, N. A. (1989). Compressor aerodynamics. Longman Scientific & Technical.